Advances in Science and Technology Research Journal

Advances in Science and Technology Research Journal, 2025, 19(7), 197–210
https://doi.org/10.12913/22998624/203976
ISSN 2299-8624, License CC-BY 4.0

Received: 2025.03.03
Accepted: 2025.05.09
Published: 2025.05.25

Cutting forces during milling of vertical thin-walled structures of aerospace alloys

Krzysztof Zagórski[1]

[1] Faculty of Mechanical Engineering and Robotics, AGH University of Krakow, al. Mickiewicza 30, 30-059 Krakow, Poland
* Corresonding author's email: zagkrzys@agh.edu.pl

ABSTRACT

The article presents the results of the experiment conducted under controlled cutting conditions with a constant material removal rate, an increased cross-section of the cutting layer was used, tested for use in finishing. The analysis examined the influence of input factors on the measured values. Samples with a thin wall in vertical orientation were made of two materials – titanium Ti6Al4V and nickel alloy Inconel 625, which were the first input factor. Additional variable factors adopted during machining were cutting tools (a general purpose tool, a tool for efficient machining, a tool for high-speed machining) and machining strategies (side face milling and cylindrical side milling). The prepared samples contain two machined surfaces – inputs and outputs. During machining, the signal of cutting force components was recorded for them, based on which their graphs were made. In the case of side face milling of nickel alloy, an approximately 50% increase in the Fx component and an approximately two-fold increase in the Fy and Fz components is observed compared to their titanium alloy counterparts. When milling titanium alloy samples, the values of the cutting force components between the strategies were similar, whereas for nickel alloy samples, milling with general-purpose and performance tools resulted in the cutting force component Fx being half as large as for the frontal approach.

Keywords: vertical thin-walled sample, milling, cutting forces, aerospace materials, titanium alloy, Ti6Al4V, nickel alloy, Inconel 625.

INTRODUCTION

The cutting process begins with the application of a sufficiently large and properly oriented force within the tool-to-workpiece system. This force is necessary to overcome the material's resistance to deformation, the frictional resistance, and the resistance to the disruption of cohesion, which allows for the creation of a new surface. The applied force separates the excess material as a chip from the workpiece [1, 2]. Ciecieląg and Zaleski [7] investigated the effect of element thickness and unsupported element on the maximum values of the vertical force for thin-walled elements made of

aluminum and titanium alloys and polymer composites. Duan et al. presented factors involved in milling process simulation and analysed milling force coefficient [8]. Jain et al. [9] found experimentally the effect of radial depth of cut during step-machining strategy of thin materials made of aluminum alloy. Bołon et al. [10] stated that high-speed milling is currently one of the key milling methods used in the aerospace industry. Huang, et al. [11] analyzed dynamic forces in milling thin-wall components with variable chip load. Liu et al. [12] proposed a position-oriented milling process monitoring model for titanium alloy Ti-6Al-4 V.

The action of the cutting force is accompanied by the cutting resistance, which is the resultant resistance of the workpiece during machining. The cutting force depends on many variable factors such as the mechanical properties of the workpiece material, the geometry of the cutting tool, the cross-sectional area of the cut layer,

and the cutting conditions and parameters, so its value can vary over a wide range [1, 3]. For this reason, it is important to select appropriate machining parameters, cutting tool and surface treatment strategy [2, 4, 5]. The effect of cutting parameters on the value of the cutting force varies. Cutting speeds have the least impact on changes in force values, whereas the depth of cut has the most significant effect. Increasing the depth of cut enlarges the cross-sectional area of the material being cut, which in turn leads to an increase in cutting forces [4, 5].

The impact of cutting forces in the milling process can cause static deflection, which depends on the machining strategy and cutting parameters [13-17]. Currently, high-speed methods reduce cutting forces, but the technology does not eliminate the deflection of the workpiece [18, 19].

The high demand for air transport forces manufacturers to increase the production of aircraft designed for passenger and cargo transport. This demand influences the search for new construction materials, solutions in the design and production of aircraft structures. One approach is to use thin-walled structures that reduce the mass of the element but provide sufficient stiffness during the occurring loads. The production of this type of elements is associated with high processing costs.

The industry strives to reduce machining costs by, among others, shortening the machining time by searching for new machining methods or increasing cutting parameters [20] One approach to increasing machining parameters is to increase the cross-section of the machined layer, which increases cutting forces and the properties of the finished product [4, 5]. Therefore, for their evaluation, determined by such quantities as surface topography or dimensional deviations, it is useful to know the phenomena occurring during the machining process [20]. They can identify the causes of inconsistencies during part execution, which can serve as a basis for improving machining conditions. [21–23]. The aforementioned phenomena can include the measurement of cutting forces. Based on their course, it is possible to determine whether the process is stable, or to look for anomalies during machining [20]. Many of the presented works are of a simulation nature, so it is necessary to conduct experiments to confirm the obtained results [6, 24]. It is observed that there is a lack of experimental research on the evaluation of cutting forces during the machining of thin-walled titanium or nickel alloy parts, so it is reasonable and necessary to conduct research in this area [26].

The purpose of the paper is to evaluate the cutting force occurring during the last full-pass (finishing) milling of thin-walled sample surfaces in a vertical orientation for a combination of input factors - workpiece material, cutting tool, and cutting strategy. It is worth mentioning that the results presented in the article are part of a larger experiment within the framework of which the influence of input parameters on output quantities was evaluated. In the aforementioned experiment, three input factors were assumed – material, cutting tool, and cutting strategies. The material used for thin-walled samples was nickel alloy Inconel 625 and titanium alloy Ti6Al4V. Machining was carried out using three different cutting tools: performance machining, general purpose, and high-speed machining. Two types of cutting strategies were used during the experiment. Side face milling and cylindrical milling were adopted when machining samples with thin walls in a vertical orientation. The experiment carried out included the measurement of vibrations and cutting forces occurring during machining, surface topography parameters, and thin wall deviations.

In paper [24], we presented selected parameters of surface topography, and thin-wall deviations were identified using an optical method, specifically through the utilization of a 3D optical scanner for Ti6Al4V titanium alloy samples. In the article [26], we presented the waveforms of the vibration signal in the form of spectrograms for Ti6Al4V titanium alloy and Inconel 625 nickel alloy samples. In the publication [27], we showed the distribution of surface topography parameters (waviness and roughness) and vertical thin wall deviation plots determined by the optical method for Inconel 625 nickel alloy samples. We presented the correlation between the results of dimensional and shape accuracy obtained through optical measurements (a 3D optical scanner was used) and contact measurements (With the use of a coordinate measuring machine) in the study [28]. The presented laboratory tests extend the scope of knowledge concerning the measurement of cutting force parameters during milling of thin-walled titanium and nickel aircraft alloys. First of all, they fill the gap in the literature regarding the selection of tools and machining methods.

MATERIALS AND METHODS

The machining conditions for samples containing a thin vertical wall are identical to the studies [25–28]. The machining parameters were selected in accordance with the tool manufacturer's recommendations regarding the material being machined (Table 2). This article only provides the basic information on machining conditions necessary to understand the concept of the described experiment.

The series of samples was made at a Mikron VCE 600 Pro machining center (Biel/Bienne, Switzerland) with iTNC 530 control software launched by Heidenhain (Traunreut, Germany).

The cutting was carried out with three different monolithic cutters for machining superalloys and titanium alloy: JS554100E2R050.0Z4-SIRA – universal cutter, JS754100E2C.0Z4A-HXT – cutter for performance machining and JH730100D2R100.0Z7-HXT – cutter for high-speed machining [34–36].

A 7x30x50 mm semi-finished part was mounted in a vice with a shank height of 10 mm, and this was mounted on a force gauge using mounting clamps (Figure 1).

Measurement of cutting forces during the machining of samples was conducted using a Kistler 9265B. three-axis piezoelectric force meter bolted to the machine table. The force meter was connected to a Kistler LabAmp Type 5165A load amplifier. The signal was recorded on a computer using dedicated Kistler LabAmp software (Figure 1).

In the experiment, we processed thin-walled samples oriented vertically, with documentation and dimensions provided in Figure 2.

The assumed test model, which includes information on input factors and output quantities, is shown in Table 1. Based on the test model, it is seen that the input factors include the workpiece material, the cutting strategy, and the cutting tool. The workpiece material was popular aerospace alloys – nickel alloy Inconel 625 and titanium

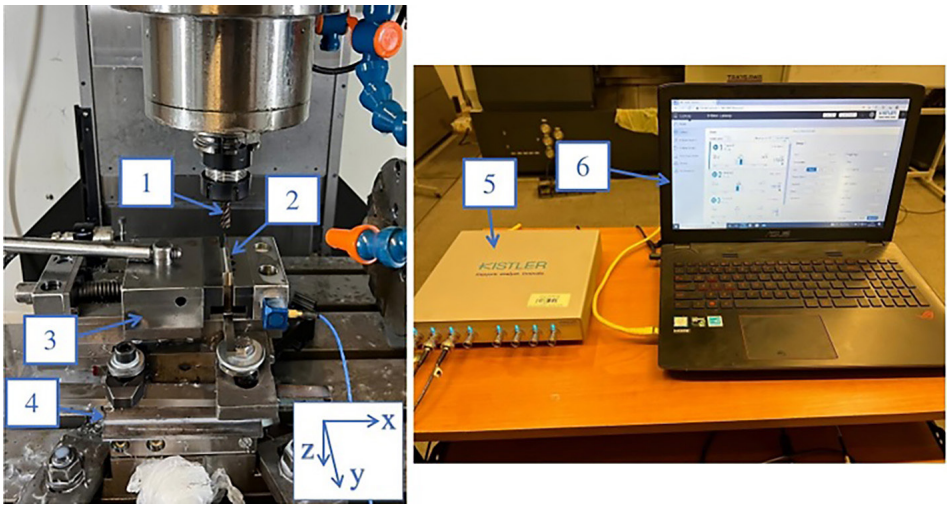

Figure 1. Experimental setup: 1 – tool; 2 – sample; 3 – vise; 4 – Kistler 9265B piezoelectric actuator; 5 – Kistler LabAmp Type 5165A load amplifier; 6 – computer with dedicated Kistler LabAmp software

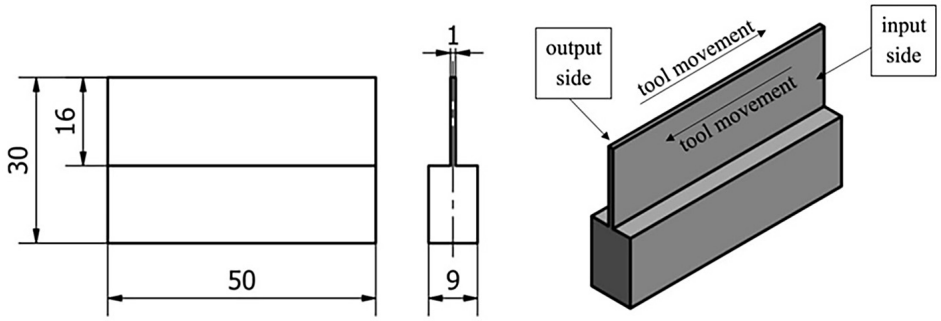

Figure 2. Documentation of the vertical thin-walled sample [26]

alloy Ti6Al4V. Inconel 625 is a nickel-chromium-molybdenum alloy with the addition of niobium, in which molybdenum increases strength (Rm 827-1103MPa) without the need for hardening by heat treatment, and is also resistant to corrosive environments. Ti6Al4V alloy class 5 (Rm 950 MPa) with 94.3%Ti, 6%Al, 4%V, 0.25%Fe and 0.2%O in the annealed condition is highly machinable and can be welded using conventional methods. Two side milling strategies were adopted - cylindrical milling and face milling and three different monolithic cutters were used for different machining methods - general-purpose high-speed, and performance machining.

The combinations of parameters and cutting conditions used are summarized in Table 2. The assumption for the selection of cutting speed and feed rate was the choice of a value contained in the middle of the range recommended by the cutting tool manufacturer. The adopted value of cutting speed v_c during the milling of titanium alloy samples is a typical value (or close to the assumed one) in studies [23–26]. Based on the presented parameters, it is evident that the value of the removal rate – which depends on the depth of cut, feed rate, and radial depth – is constant and equals 2.03 cm^3/min. Using a constant value for this parameter was the basis for comparing the results. During machining, SILUB MAX water-oil emulsion cooling was applied in a proportion of 85% water and 15% oil [27].

The measurement of cutting forces for each sample was recorded on three components F_x, F_y, F_z marked according to the coordinate system shown in Figure 1. A sampling frequency of 1000Hz was used during the measurement. To determine the values of the component forces, it was necessary to set the appropriate sensitivities of the force meter, which were selected according to the datasheet provided by the manufacturer of the force meter used. The sensitivities adopted for calibration of the force meter are shown in Table 3.

RESULTS AND DISCUSSION

The cutting force components along the three axes of the coordinate system (x, y, z) during the machining process of the samples were determined based on the conditions described before. These components are designated as Fx, Fy, and Fz, respectively. For parts with thin vertical walls, the cutting force component F_x is the normal feed force, the F_y component is the feed force, and the F_z component is the resistance

Table 1. The assumed research model

Input factors	Test object	Output factor
• Workpiece materials, • Cutting tools (for different milling methods), • Machining strategies.	• Thin wall samples in horizontal orientation	• Cutting forces

Table 2. Cutting parameters adopted during the experiment (based on [34–36])

Sample number	Material	Cutting tool	Machining strategy	a_p [mm]	a_e [mm]	V_c [m/min]	V_f [mm/min]
T1_1	Titanium alloy Ti6Al4V - grade 5	JS554100E2R050.0Z4-SIRA	Face side milling	2	4	100	255
T2_1		JS754100E2C.0Z4A-HXT		2	4	100	255
T3_1		JH730100D2R100.0Z7-HXT		2	4	100	255
T4_1		JS554100E2R050.0Z4-SIRA	Cylindrical side milling	16	0.5	100	255
T5_1		JS754100E2C.0Z4A-HXT		16	0.5	100	255
T6_1		JH730100D2R100.0Z7-HXT		16	0.5	100	255
N1_1	Nickel alloy Inconel 625	JS554100E2R050.0Z4-SIRA	Face side milling	2	4	40	255
N2_1		JS754100E2C.0Z4A-HXT		2	4	40	255
N3_1		JH730100D2R100.0Z7-HXT		2	4	40	255
N4_1		JS554100E2R050.0Z4-SIRA	Cylindrical side milling	16	0.5	40	255
N5_1		JS754100E2C.0Z4A-HXT		16	0.5	40	255
N6_1		JH730100D2R100.0Z7-HXT		16	0.5	40	255

Table 3. Calibration data for the Kistler 9265B dynamometer (based on manufacturer's documentation)

Cutting force component	Calibration range [N]	Sensitivity [pC/N]
F_x	0 – 15000	–7.86
F_y	0 – 15000	–7.91
F_z	0 – 30000	–3.6

force. Consequently, considering the axes of the machine tool coordinate system, the transitions on the input side had positive values of cutting forces on the x, and y components, while on the output side, the values of these components were negative. It is due to a change in the direction of the force – milling on the output side took place in the opposite direction on the x and y axes than on the input side. The cutting force component along the z-axis was positive for both the entry and exit of the tool from the material.

Using the recorded measurement results from a piezoelectric force gauge with a sampling frequency of 1000 Hz, a graphical representation of the cutting force components on the three axes of the coordinate system for the last complete pass on both the input and output sides was developed in the Matlab program.

Cutting force for titanium alloys samples

The graphs of the cutting force components of the last pass for titanium alloy samples with thin vertical walls manufactured using face side milling are shown in Figure 3a-c, while Figure 3d-f was obtained using cylindrical side milling.

Based on the graphs shown in Figure 3, it is reported that for samples made with the tool for high-performance machining and the tool for general purposes, we observe that both their shape and the accepted values of the corresponding components of the cutting forces are similar to each other. This relationship applies to the comparison of samples performed using side face milling with cylindrical milling, i.e. the comparison of T1_1 and T2_1 and T4_1 and T5_1. The trend works for both sides machined, i.e., No significant differences were observed between the input and output sides of the samples T1_1, T2_1, T4_1, and T5_1 (3%). The similar nature of the graphs of the corresponding components of the cutting forces may be due to the similar geometry of the two cutters. As mentioned, the values of the corresponding components for the opposite strategies are similar to each other, but slightly smaller values (mainly of the F_y component) were registered for the samples made with the side face milling strategy (T1_1 and T2_1) was 3% and the cylindrical one (T4_1 and T5_1). The decrease in cutting force is because in this strategy the thin wall has no support from the other side, so it can be deflected by the pressure of the milling cutter during machining, and as a result deform.

The differences in cutting force components between the machining strategies applied to samples produced using the general-purpose tool (T1_1 and T4_1) was 3% and the high-performance machining tool (T2_1 and T5_1) are negligible. However, this is not the case for samples manufactured with the high-speed machining tool (T3_1 and T6_1). Notably, sample T3_1, which was processed with the high-speed machining tool in conjunction with the side face milling strategy, exhibits a distinct graph pattern, characterized by significantly higher cutting force component values components by 30% compared to the other samples made with the same strategy (T1_1 and T2_1). The different character is characterized by a different location of peaks, sample T3_1 presents peaks at the beginning of the transition for both sides - input and output - on the x and z axes. For samples T1_1 and T2_1, the observed peaks appear at the beginning of the transition and are only present on the output side along the y-axis. Additionally, when utilizing the high-speed machining tool, the cutting force components recorded for side face milling (T3_1) were notably higher compared to cylindrical milling (T6_1), which contrasts with the trend observed for samples processed with the general-purpose and high-performance machining tools. Upon examining the graphs obtained during machining with the high-speed tool, it becomes evident that the cutting forces for the sample produced using the cylindrical side milling strategy (T6_1) are up to twice as low as those recorded for the face milling strategy (T3_1). Sample T6_1 exhibits a graph pattern similar to other samples subjected

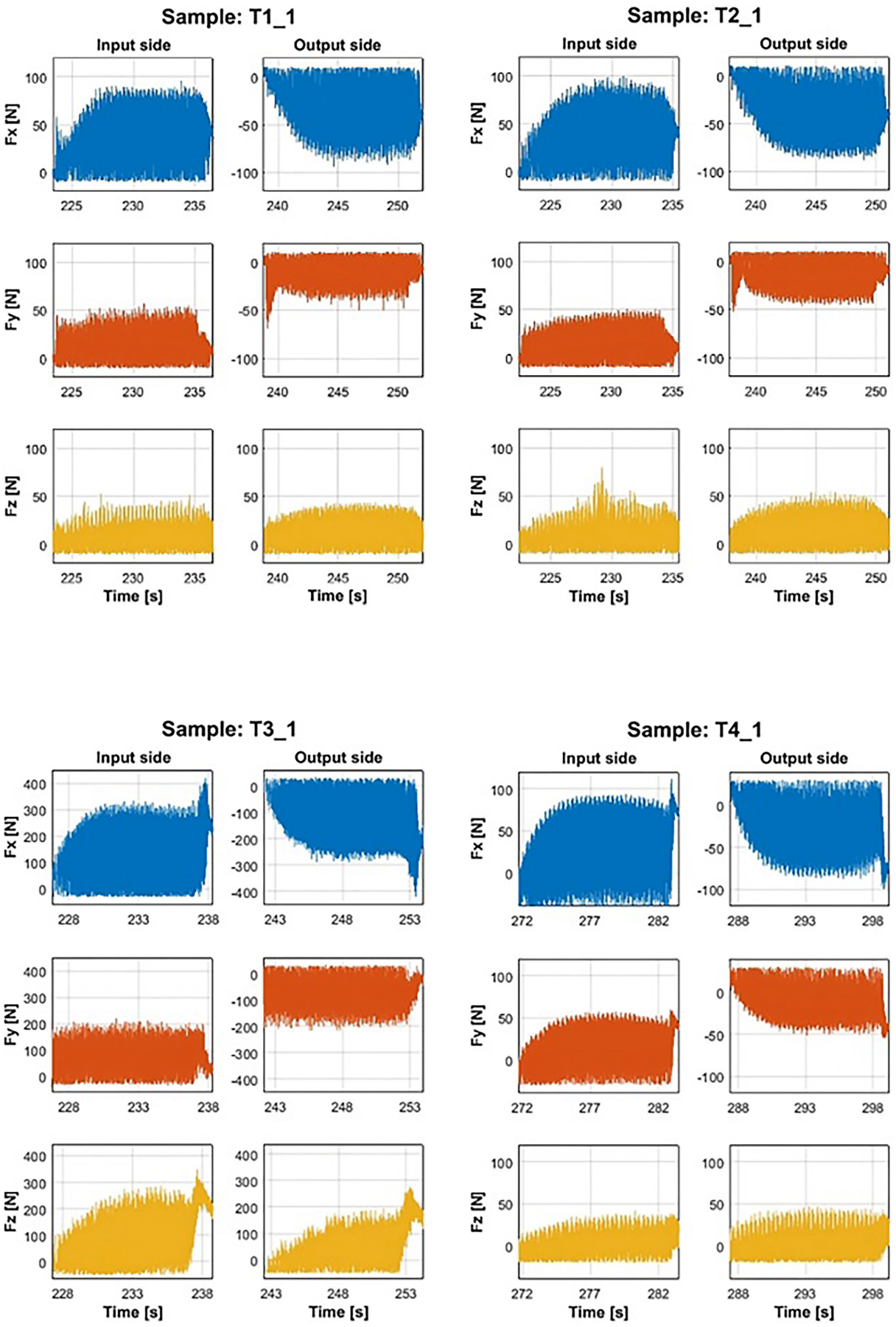

Figure 3. The components of the cutting force for the sample: (a) T1_1; (b) T2_1; (c) T3_1; (d) T4_1; (e) T5_1; (f) T6_1

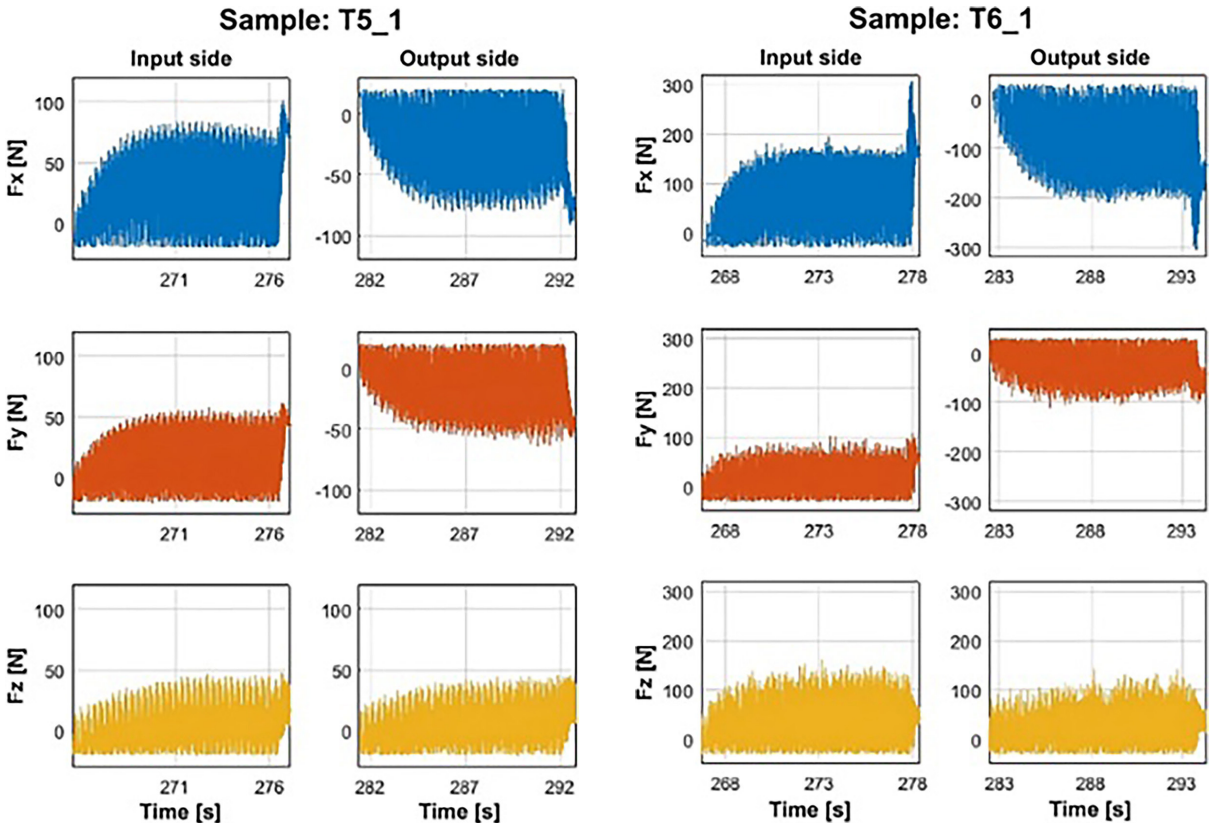

Figure 3 cont. The components of the cutting force for the sample: (a) T1_1; (b) T2_1; (c) T3_1; (d) T4_1; (e) T5_1; (f) T6_1

to the same strategy (T4_1 and T5_1), but with significantly higher cutting force component values and a considerably larger peak increase at the end of the x-axis transition.

For the side face milling strategy, a slightly higher instability is observed, i.e. the graph is rough, as the tool is forced to overcome a lot of resistance during cutting. An additional factor is that during side face milling, the force is concentrated on a larger arm from the mounting holder compared to the opposite strategy, so it is more sensitive to component vibration that occurs.

The application of the side cylindrical milling strategy (T4_1 – T6_1) provides more stable graphs, i.e. without sudden peaks (increases in cutting forces). The exception is the occurrence of a peak at the end of each pass for all tools used, the strong influence of which is noticeable on the x-axis (direction normal to the feed motion), and a less significant impact is observed on the y-axis, which represents the direction of the feed motion. The peaks appear to result from the need to overcome the resistance to material breakage during tool exit.

Cutting force for nickel alloys samples

In the next step, results were developed for samples machined from nickel alloy, whose graphs of the components of the cutting forces were prepared in the same way as for titanium alloy. First, graphs were determined for samples made by the side face milling strategy (N1_1 – N3_1), which are shown in Figure 4a-c. Following this, plots of the component cutting forces of samples machined with the cylindrical side milling strategy (N4_1 – N6_1) were prepared, which are shown in Figure 4d-f.

Similar to the titanium alloy, the cutting force component plots for nickel alloy samples machined using the general-purpose tool (N1_1 and N4_1) and the high-performance machining tool (N2_1 and N5_1) exhibit comparable patterns across the individual component axes. A mutual comparison of the samples obtained with these two tools in terms of strategy shows that the corresponding values of the component cutting forces - the component cutting forces of samples N1_1 and N2_1 and N4_1 and N5_1 – are comparable to each other and the difference in results

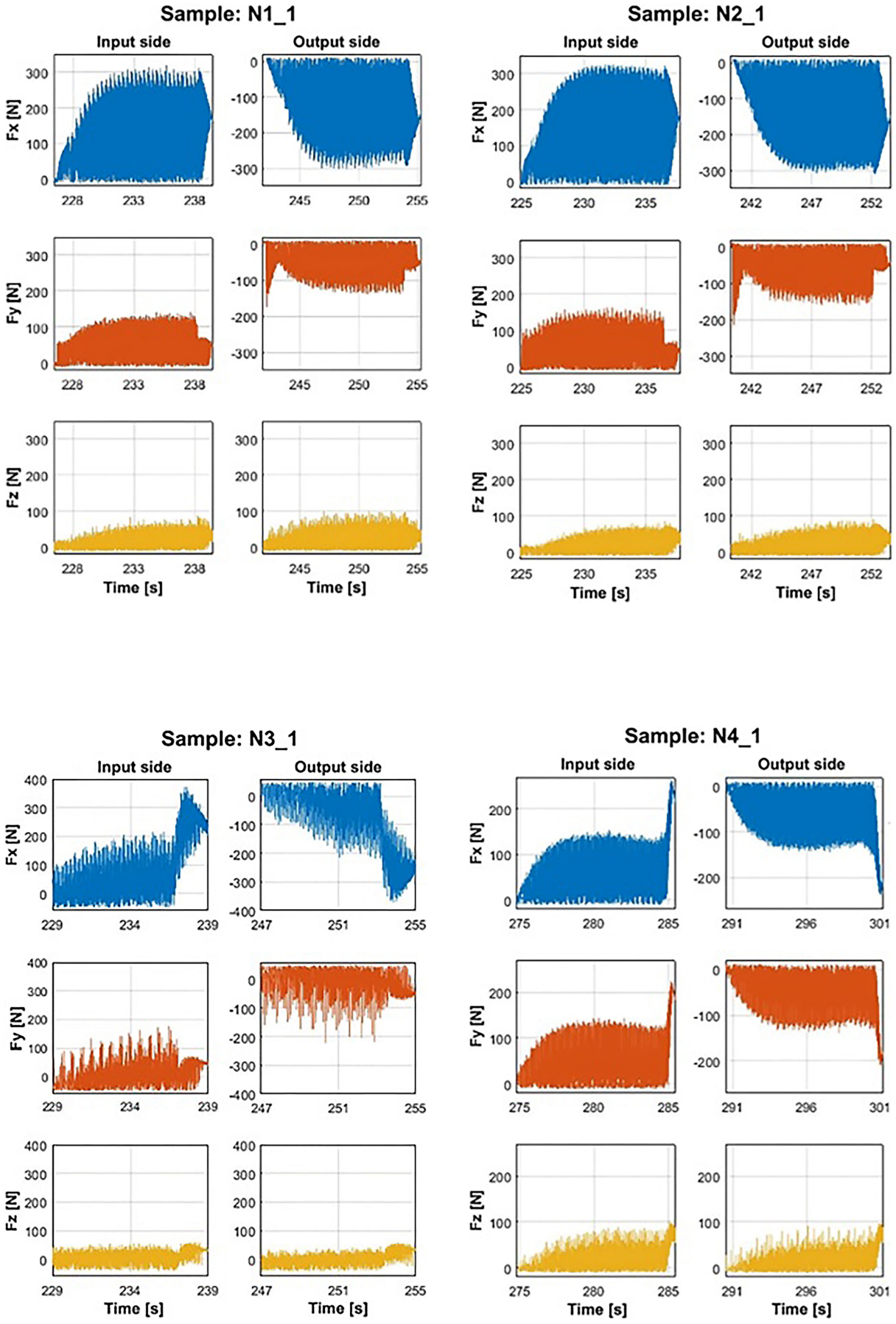

Figure 4. The components of the cutting force for the sample: (a) N1_1; (b) N2_1; (c) N3_1; (d) N4_1; (e) N5_1; (f) N6_1

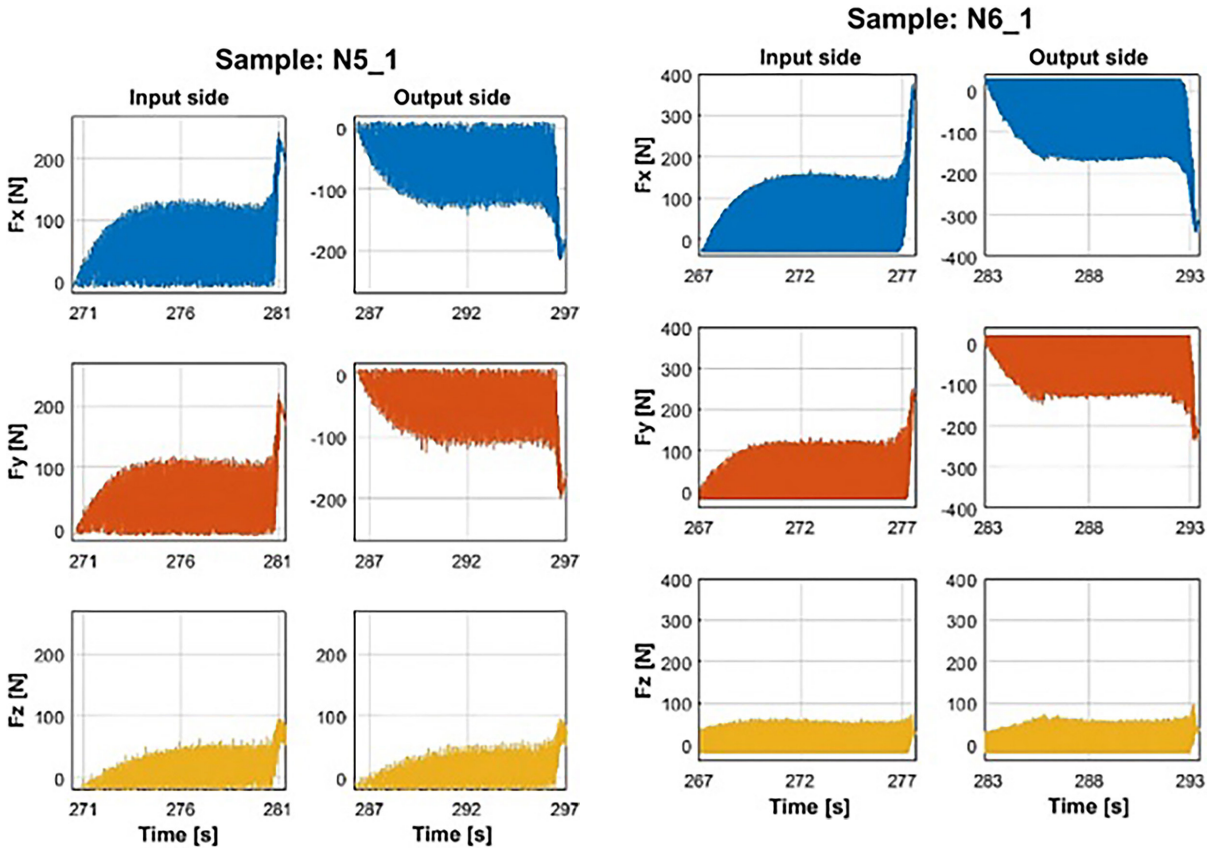

Figure 4 cont. The components of the cutting force for the sample: (a) N1_1; (b) N2_1; (c) N3_1; (d) N4_1; (e) N5_1; (f) N6_1

was about 10%. This is a result of the similar geometry of the two tools, which translates into similar conditions in terms of the achieved cutting forces, which was also observed in the graphs of the titanium alloy samples.

Analyzing the values of the cutting force components of the nickel alloy samples, it is evident that for those obtained with the side face milling strategy (N1_1 and N2_1), an approximately 50% increase in the F_x component and an approximately twice as much increase in the F_y and F_z components is observed compared to their titanium alloy counterparts (T1_1 and T2_1). The samples machined with the cylindrical side milling strategy (N4_1 and N5_1) show about three times the values of the F_x component and about twice the increase in the F_y and F_z components compared to their titanium alloy counterparts (T4_1 and T5_1). The increase in cutting forces was expected because nickel alloy is a significantly harder material compared to titanium alloy. so a higher force is required to break the material during machining.

When milling titanium alloy samples, the values of cutting force components between strategies were similar. For nickel alloy samples made with the tool for general purpose and high-performance machining, half the values of the F_x component were obtained during cylindrical side milling (N4_1 and N5_1) compared to face milling (N1_1 and N2_1). This statement is correct when the peaks at the end of the transition for this component are ignored.

For the components F_y and F_z, the cutting force values were about 25% higher for cylindrical side milling (N4_1 and N5_1) compared to face milling (N1_1 and N2_1). The observations presented lead to the conclusion that the harder material, as well as the strategy used, affected the increase in values and the change in the distribution of the cutting force among the components.

Focusing on the peak values of the samples described above, we see that in the case of samples N1_1 and N2_1, it is observed that there is a peak at the beginning of the transition on the y-axis on the output side – with a similar increase (about 50%) as in the case of titanium alloy. Peaks at the end of the transition on both sides machined for samples N4_1 and N5_1 are seen on

all components – as in the case of their titanium alloy counterparts. However, the aforementioned peaks tend to increase more compared to titanium alloy, as up to twice as much is observed when comparing them to the obtained cutting forces in the right part of the transition.

Samples were obtained using a tool specifically designed for high-speed machining. (N3_1 and N6_1) present different trends. Focusing on sample N3_1, made with the side face milling strategy, it is apparent that it showed a different character than the other samples obtained with the same strategy in both nickel alloy and titanium alloy. The course of the components of the N3_1 sample tends to be more unstable, manifested by a rough graph, i.e. sudden increases in the values of cutting forces. Interestingly, a very regular graph is noted when the same tool is used, but with a cylindrical side milling strategy (N6_1) – meaning that the smoothest graph was obtained in the group of titanium and nickel alloy samples. The graph itself and the nature of the graph for sample N6_1 are similar to the graphs obtained with other tools with the same strategy (N4_1 and N5_1) but with a smoother and more regular course of values. A similar situation occurs for the obtained values of the components of the cutting forces, ignoring the values of the peaks occurring at the end of the transition, which are larger.

An interesting situation is observed by focusing on the comparison of values for nickel and titanium alloy samples made with the tool for high-speed machining. The results presented for N3_1 and N6_1 are similar in value to those obtained for sample T6_1 (titanium alloy, cylindrical side milling) and about half the value for T3_1 (titanium alloy, face side milling). The nickel alloy selected for this study is harder than the titanium alloy, so an increase in cutting forces was expected when machining it compared to titanium—which was confirmed for samples processed with the general-purpose and high-performance machining tools. However, this trend was not observed when using the high-speed machining tool on nickel alloy. It was noted that, for titanium alloy samples, the cutting force components were twice as high for those machined with the high-speed tool using a side face milling strategy (T3_1) compared to cylindrical milling (T6_1). In contrast, when machining nickel alloy, the use of this tool resulted in similar cutting force values for both strategies (N3_1 and N6_1). These findings highlight the significant influence of material properties on the machining process when using the high-speed machining tool under these conditions, where a harder material appears to reduce cutting forces.

Statistical analysis of cutting forces

For the statistical analysis conducted for samples with thin horizontal walls, the maximum values of the total cutting force F_c for all passes were assumed, determined by vector compositing of the selected components F_x, F_y, and F_z. Figures 5 and 6 show the mean values, standard error, and standard deviation for titanium alloy and nickel alloy samples, respectively. Appendix A contains Table A1 with the minimum and maximum values, mean, median, variance, standard deviation, and standard error for the analysis.

Based on the Figures 5 and 6 graphs, showing the values of the total cutting force F_c for titanium and nickel alloy samples, the following observations can be given:

The application of the tool for general purpose (T1_1 and T4_1) and the tool for high-performance machining (T2_1 and T5_1) is characterized by similar mean value 121.55N and 13.99N and scatter of results for titanium alloy samples made under the same conditions (for both cutting strategies).

It is impossible to clearly determine which strategy yielded more favorable results based on the presented data. For the tool for general purposes (T1_1, T4_1, N1_1, and N4_1) and the tool for high-performance machining (T2_1, T5_1, N2_1, and N5_1), the average values are similar. For the tool for high-speed machining, in the titanium alloy group (T3_1 and T6_1), smaller average values were obtained for the cylindrical side milling strategy by 8% compared to the face milling strategy, while in the nickel alloy group (N3_1 and N6_1), the trend is the opposite – smaller average values were obtained for the face milling strategy compared to the face milling strategy by 10%.

Comparing the values of the total cutting force F_c depending on the workpiece material, similar to the above observation on strategy, also yields inconclusive results. For samples machined with the tool for general purposes and the tool for high-performance machining, smaller values were obtained for titanium alloy compared to nickel alloy. For the tool for high-speed machining, smaller values were obtained for titanium alloy with the cylindrical side milling strategy, while for nickel

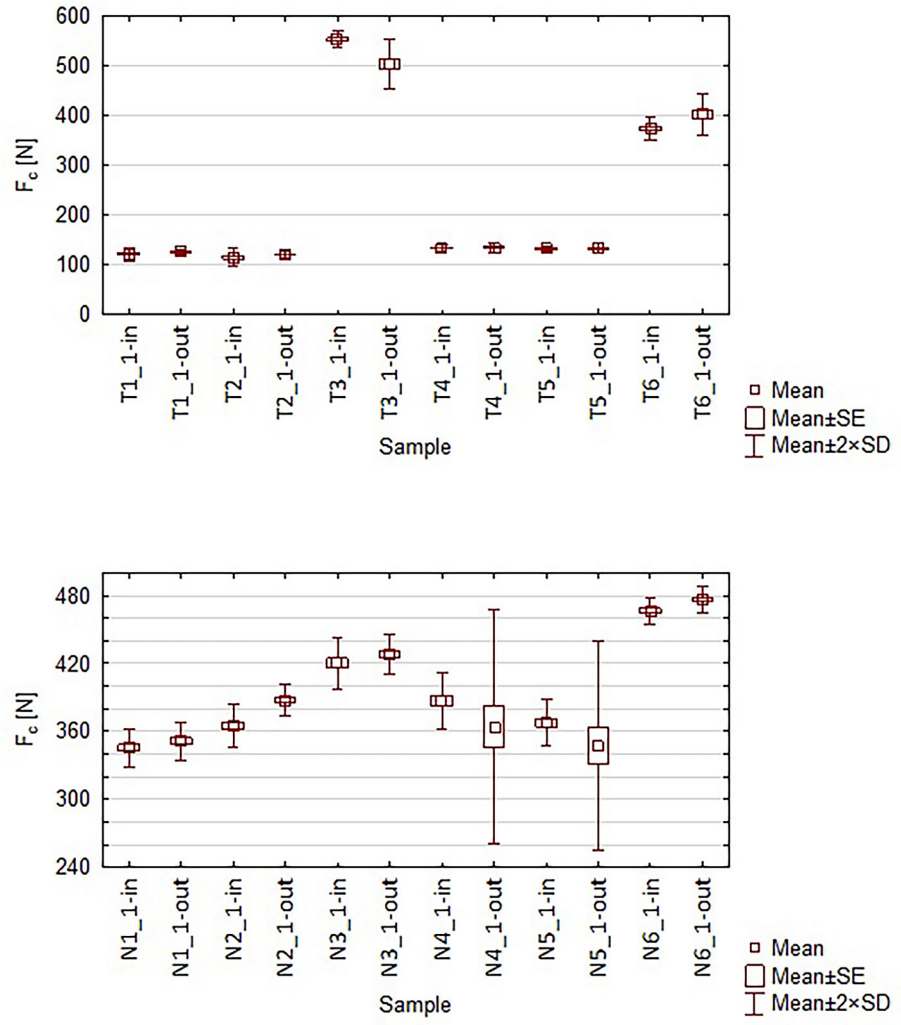

Figure 6. The results of total cutting force statistics for nickel alloy samples

alloy, the sample was machined with the face milling strategy.

Both in the titanium alloy group and in both material groups, the largest average value was observed for sample T3_1 – 1 552.77N, while the smallest was for T2_1 – 114.27N (with similar values for T1_1, T4_1, and T5_1).

In the nickel alloy group, the highest mean value was observed for sample N6_1 – 466.68N, while the lowest was for N1_1 – 345.65N (with similar values for N2_1, N4_1, and N5_1).

The use of the tool for general purposes and the tool for high-performance machining gives similar values of cutting forces, potentially due to similar cutter geometries. Machining with the tool for high-speed machining presents significantly higher values of the obtained cutting forces.

Figures 7 and 8 show the results of statistical analysis of the significance of two side milling parameters on the entry and exit side for two machined materials. Vertical bars indicate 0.95 confidence intervals. The results were processed using the ANOVA method in Statistica.

Comparing the significance levels between the input side and output side for titanium and Inconel materials, it can be concluded that the average values of total cutting force do not show significant difference.

CONCLUSIONS

This paper presents the cutting force results for machining of titanium alloy Ti6Al4V and nickel alloy Inconel 625 for three different tools (general purpose, high performance and HSM) and milling strategies – side and side milling.

Based on the results of this study, the following conclusions can be drawn:

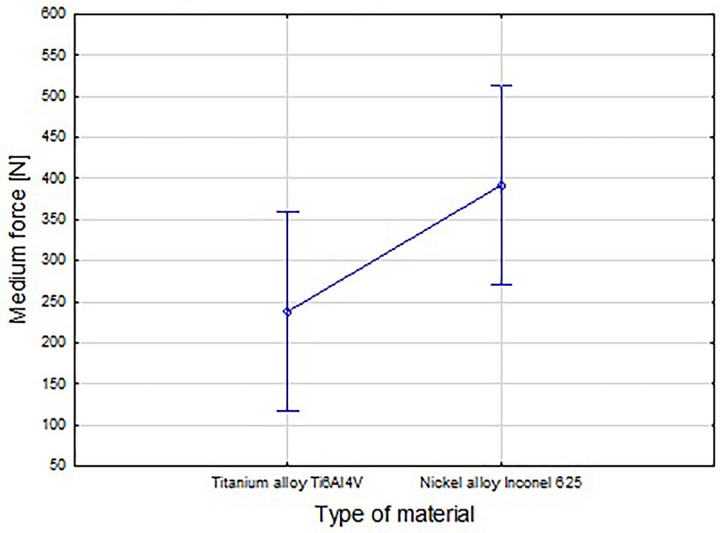

Figure 7. Side milling severity levels on the entry side, (F = 3.9827, p = 0.07392)

- For most of the samples, approximately 50% lower average values of total cutting force were obtained when milling titanium alloy samples.
- It is not possible to clearly state which machining strategy resulted in lower cutting forces, because the results depend on the tools used.
- The average values of total cutting force are very similar for samples made with the general purpose tool and the high performance tool (3%) – in terms of material. This trend is very visible in the results obtained when machining titanium alloy samples.
- The use of a high-speed cutting tool showed that in the case of the titanium alloy, lower values were obtained by using the cylindrical side milling strategy, while in the case of the nickel alloy, lower values were obtained by using the side milling strategy by 30%, while in the case of the nickel alloy, lower values were obtained by using the side milling strategy.
- The lowest value of the total cutting force (taking into account both analyzed material groups) was obtained for sample T2_1 – 114.27 N of the titanium alloy machined with a high-performance cutting tool using side milling.
- The highest value of the total cutting force (taking into account both analyzed material groups) was obtained for sample T3_1 – 552.77 N of the titanium alloy machined with

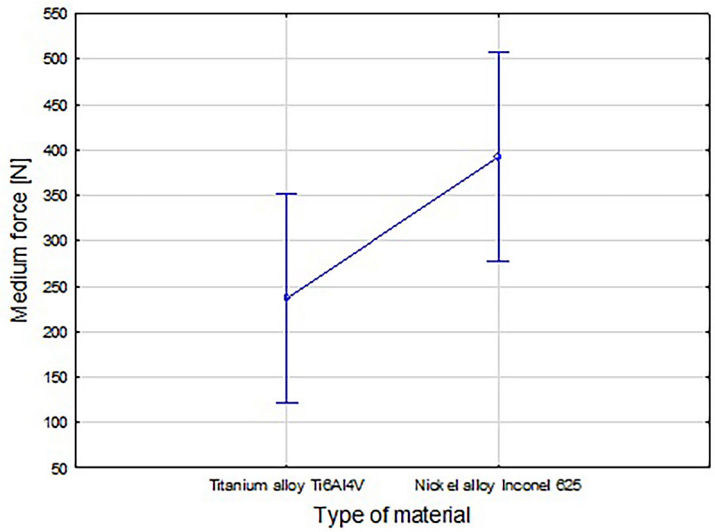

Figure 8. Side milling severity levels on the exit side, (F = 4.5871, p = 0.05786)

a high-speed cutting tool using side milling. An interesting observation is that lower results were obtained when machining the nickel alloy corresponding to this sample – N3_1 – 420.55 N (the same cutting conditions)..

Based on the overall research conducted, the following possible directions for research can be done:

- Machining samples with different thin wall thicknesses and controlling parameters.
- Using different combinations of cutting speed and feed rate, as well as cutting depth and radial depth to determine the favorable values.
- Using different support methods to minimize the effects of vibration and cutting forces.

The statistical results of cutting forces for thin wall samples in a vertical orientation are presented in Appendix (Table A1), comparing titanium alloy and nickel alloy.

REFERENCES

1. Dul-Korzyńska, B. Obróbka skrawaniem i narzędzia; Oficyna Wydawnicza Politechniki Rzeszowskiej: Rzeszów, Poland, 2005.
2. Kaczmarek, J. Podstawy obróbki wiórowej, ściernej i erozyjnej; Wydawnictwo Naukowo-Techniczne: Warszawa, Poland, 1971.
3. Kiszka, P. Badanie mechanicznych i termicznych oddziaływań w skrawaniu żeliwa sferoidalnego ostrzami z ceramiki azotkowej i CBN, PhD thesis, Politechnika Opolska, Opole, 2012.
4. Dmochowski, J. Podstawy obróbki skrawaniem; Wydawnictwo Naukowo-Techniczne: Warszawa, Poland, 1983.
5. Grzesik, W. Podstawy skrawania materiałów metalowych; Wydawnictwo Naukowo-Techniczne: Warszawa, Poland, 2010.
6. Jemielniak, K. Automatyczna diagnostyka stanu narzędzia i procesu skrawania; Oficyna Wydawnicza Politechniki Warszawskiej, Warszawa 2002.
7. Ciecieląg, K.; Zaleski, K. Milling of three types of thin-walled elements made of polymer composite and titanium and aluminum alloys used in the aviation industry. Materials 2022, 15, 5949.
8. Duan, Z., Li, C., Ding, W. et al. Milling force model for aviation aluminum alloy: Academic insight and perspective analysis. Chin. J. Mech. Eng. 2021, 34, 18.
9. Jain, A.K., Narasaiah, K., Gopinath, S. Machining of thin walls and thin floor aerospace components made of aluminum alloy with high aspect ratio. Materials Science Forum. 2015, 830–831, 112–115.
10. Bołon, P., Rejman, E., Smusz R., Kiełbasa B. High speed machining of the thin-walled aircraft constructions. MECHANIK 2017, 8–9, 726–229.
11. Huang, P.L., Li, J.F., Sun, J., Zhou, J. Study on performance in dry milling aeronautical titanium alloy thin-wall components with two types of tools. Journal of Cleaner Production, 2014, 67, 258–264.
12. Liu, D., Luo, M., Urbikain Pelayo, G., Olvera Trejo, D., Zhang, D. Position-oriented process monitoring in milling of thin-walled parts. Journal of Manufacturing Systems, 2021, 60, 360–372.
13. Wan, M., Zhang, W.H., Qin, G., Wang, Z.P. Strategies for error prediction and error control in peripheral milling of thin-walled workpiece. International Journal of Machine Tools and Manufacture 2008, 48, 1366–1374.
14. Li, M., Huang, J., Ding, W., Liu, X., Li, L. Dynamic response analysis of a ball-end milling cutter and optimization of the machining parameters for a ruled surface. Proceedings of the Institution of Mechanical Engineers Part B: Journal of Engineering Manufacture 2019, 233, 588–599.
15. Yan, Q., Luo, M., Tang, K. Multi-axis variable depth-of-cut machining of thin-walled workpieces based on the workpiece deflection constraint. CAD Computer-Aided Design 2018, 100, 14–29.
16. Aijun, T., Zhanqiang, L. Deformations of thin-walled plate due to static end milling force. Journal of Materials Processing Technology 2008, 206, 345–351.
17. Wan, M.; Zhang, W. Calculations of chip thickness and cutting forces in flexible end milling. The International Journal of Advanced Manufacturing Technology 2006, 29, 637–647.
18. Li, S., Zhao, W., Li, L., He, N., Chi, S. Modeling and application of process damping in milling of thin-walled workpiece made of titanium alloy. Shock and Vibration 2015, 2015(2), 1–12.
19. Tang, A., Liu, Z. Three-dimensional stability lobe and maximum material removal rate in end milling of thin-walled plate. The International Journal of Advanced Manufacturing Technology 2009, 43, 33–39.
20. Kurpiel, S., Cudok, B., Zagórski, K., Cieślik, J., Skrzypkowski, K., Brostow, W. Influence of tools and cutting strategy on milling conditions and quality of horizontal thin-wall structures of titanium alloy Ti6Al4V. Sensors 2023, 23, 9905. https://doi.org/10.3390/s23249905
21. Tran, M.Q., Liu, M.K. Chatter Identification in End Milling Process Based on Cutting Force Signal Processing. IOP Conf. Ser. Mater. Sci. Eng 2019, 654, 012001.
22. Liu, X., Jin, L. Experimental investigation into the effect of chatter on surface microtopography of

gears in grinding. J. Mech. Eng. Sci. 2016, 231, 294–308.

23. Yang, M., Mao, X., Peng, Y., Li, B., Jiang, X., Li, L. Trajectory Dependent Structural Vibration and Its Effects on Surface Generation. IOP Conf. Ser. Mater. Sci. Eng. 2019, 491, 012009.
24. Tang, J., Deng, C., Chen, X., Zhai, H. Analysis and optimization of milling deformations of TC4 alloy thin-walled parts based on finite element simulations. Machines 2023, 11, 628. https://doi.org/10.3390/machines11060628
25. Kurpiel, S., Zagórski, K., Cieślik, J., Skrzypkowski, K. Investigation of selected surface topography parameters and deformation during milling of vertical thin-walled structures from titanium alloy Ti6Al4V. Materials 2023, 16, 3182.
26. Kurpiel, S., Zagórski, K., Cieślik, J., Skrzypkowski, K., Brostow, W. Evaluation of the vibration signal during milling vertical thin-walled structures from aerospace materials. Sensors 2023, 23, 6398.
27. Kurpiel, S., Zagórski, K., Cieślik, J., Skrzypkowski, K., Tuleshov, A. Evaluation of the surface topography and deformation of vertical thin-wall milled samples from the nickel alloy Inconel 625. Materials 2024, 17, 295. https://doi.org/10.3390/ma17020295
28. Kurpiel, S., Zagórski, K., Cieślik, J., Skrzypkowski, K., Kapayeva, S., Torekhanova, M. Dimensional deviations of horizontal thin wall of titanium alloy Ti6Al4V determined by optical and contact methods. Materials 2023, 16, 7272. https://doi.org/10.3390/ma16237272
29. Yanis, M., Mohruni, A.S., Sharif, S., Zahir, M. Experimental Vibration Study in Milling Thin-Walled Ti6Al4V under MQL using Coconut Oil as Cutting Fluid. Journal of Physics: Conference Series 2020, 1500, 012034, 1-8.
30. Hintze, W., Wenserski, R., Junghans, S., Möller, C. Finish machining of Ti6Al4V SLM components under consideration of thin walls and support structure removal. Procedia Manufacturing 2020, 48, 23, 485–491.
31. Zha, J., Liang, J., Li, Y., Zhang, H.; Y. Chen, Y. Large Cutting Depth and Layered Milling of Titanium Alloy Thin-Walled Parts. Materials 2020, 13, 1499.
32. Wang, J., Ibaraki, S., Matsubara, S. A cutting sequence optimization algorithm to reduce the workpiece deformation in thin-wall machining. Precision Engineering 2017. 50, 506–514.
33. SIS Industry Catalog. Available online: https://www.sisindustry.com/chemia-przemyslowa/srodki-smarne-do-obrobki-metali/ (accessed on 07 January 2024).
34. Seco Tools Catalog—JS554100E2R050.0Z4-SIRA. Available online: https://www.secotools.com/article/p_03029964 (accessed on 07 January 2024).
35. Seco Tools Catalog—JS754100E2C.0Z4A-HXT. Available online: https://www.secotools.com/article/p_03186836 (accessed on 07 January 2024).
36. Seco Tools Catalog—JH730100D2R100.0Z7-HXT. Available online: https://www.secotools.com/article/p_03127380 (accessed on 07 January 2024).